Composites: Part A 198 (2025) 109165

Contents lists available at ScienceDirect

Composites Part A

journal homepage: www.elsevier.com/locate/compositesa

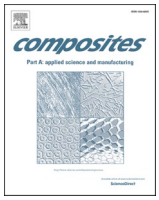

Upcycling of unidirectional carbon-fibre/PEEK prepreg trim waste

A.W. Smith [a], H. Pattery [a], J.P. Canart [c], I. Tabiai [a,b], M. Dubé [a,b,*]

[a] Mechanical Engineering, École de technologie supérieure, Montréal, Canada
[b] Research Center for High Performance Polymer and Composite Systems (CREPEC), Québec, Canada
[c] Teijin Carbon America Inc., Rockwood, United States

ARTICLE INFO

Keywords:
Recycling
Thermoplastic composites
Strand-based composites

ABSTRACT

During manufacturing of unidirectional thermoplastic prepregs, the material edges are trimmed as they feature unacceptable variations in thickness and resin content. This tape edge trim (TET) is chopped into pieces before exiting the prepregging line to facilitate disposal. This process produces a material resembling strand-based compounds referred to in the literature as randomly orientated strands. However, the chopping operation produces TET with a broad range of geometries making direct reuse by compression moulding likely to produce components with uncertain mechanical properties. Here, two different sieving methods are used to sort carbon fibre TET into batches with more consistent geometries. Sieving involving linear vertical agitation is found to result in less strand damage and overall efficient sorting compared to sieving that involves in-plane agitation. The sorted TET is compression moulded into panels which are characterized by ultrasonic inspection, microscopy and mechanical testing. A general increase in the average tensile and flexural strengths is observed for the panels manufactured using TET recovered from the largest sieves, *i.e.*, having a higher average strand length. However, the variability of the mechanical properties remains. A brief analysis of the environmental impact of reusing the TET instead of virgin strands is presented.

1. Introduction

The manufacture of thermoplastic prepregs, also known as *prepregging*, involves the impregnation of dry fibre tows with molten or softened polymer at elevated temperatures and pressures, typically using heated rollers. This process provides excellent control over both thickness and resin-to-fibre ratios across most of the prepreg surface. However, these characteristics can become non-uniform near the prepreg edges, which must then be trimmed prior to rolling. The trimming biproduct, referred to here as tape edge trim (TET) waste, is cut into strands during prepregging to minimize production stoppages and facilitate disposal. Fig. 1 shows a sample of TET waste collected from the prepregging line of Teijin Carbon America Inc., an aerospace material supplier.

Despite not satisfying the quality requirements for primary aerospace structures, TET consists of high-performance constituent materials such as standard or intermediate modulus Tenax® carbon fibre, as well as a variety of thermoplastic polymer systems (e.g., polyetheretherketone (PEEK), polyetherketoneketone (PEKK), polyphenylene sulfide (PPS), low-melt polyaryletherketone (LM-PAEK) or polyetherimide (PEI)). To dispose of this waste via traditional methods such as landfilling would be to lose a high-value material with little contamination, while contributing to the overwhelming environmental problem of plastic pollution. Notably, TET waste currently represents up to 15 % of the prepreg roll's weight, depending on factors such as roll width and process optimization levels achieved during a given production cycle.

TET waste strongly resembles a number of commercially available strand-based compression moulding compounds such as Toray's Cetex® MC1200 [1]. Halfway between continuous fibre and discontinuous short-fibre composites, these strand-based composites offer a compromise between processability and performance. Increasingly present in industry [2], they are made of rectangular flakes of varying lengths (e.g. 12.7 mm, 25.4 mm or 50 mm) cut from prepreg rolls. Literature shows that both strength and modulus increase with the length of the strands, and therefore the fibre length [3–6]. This trend, observed in both thermoset [4] and thermoplastic composites [5], is limited beyond a certain length as observed by Eguémann [3] and Yamashita [6] in their tensile test results. Changing fibre length generally has more of an impact on composite strength, rather than modulus [3,4,7]. The effect of the strand width is not as consistent. For a same strand length, a higher strength is

* Corresponding author.
E-mail address: martine.dube@etsmtl.ca (M. Dubé).

https://doi.org/10.1016/j.compositesa.2025.109165
Received 25 March 2025; Received in revised form 15 June 2025; Accepted 5 July 2025
Available online 6 July 2025

Fig. 1. TET waste from Teijin Carbon America Inc. which has been chopped into strands following polymer impregnation.

obtained when increasing the strand width from 4.1 mm to 8.4 mm, according to Feraboli [4]. However, comparing tensile results of specimens made from 12.7 mm square strands against 12.7 mm (length) x 1.59 mm (width) rectangular strands, Tomblin [8] found better performance for the latter dimension. Finally, Selezneva [9] found that varying the strand width between 12 and 50 mm, while maintaining a strand length of 25 mm, had no effect on coupon tensile properties. Generally, a high variability is observed for all data.

The majority of reported failure modes are matrix-dominated [3,4]. Selezneva [5] notes that this matrix failure mode could explain the lower strength values reported for specimens made from shorter strands. In effect, resin rich areas are more frequent in laminates made from smaller strands, increasing the number of potential locations where failure can occur.

Because TET waste consists of strands with a much broader range of geometries than is typical of commercial compounds, it is reasonable to assume *a priori* that having strands of various sizes within the same compound may increase mechanical property variability, leading to additional challenges with material qualification for structural applications.

The aim of this work is to evaluate the feasibility of recycling TET waste through compression moulding, while considering mechanical performance and cost-volume factors. First, the geometric homogeneity of recovered TET waste is improved using two mechanical sieving methods. Then, sorted TET batches featuring progressively smaller strands are used to compression mould simple panels for mechanical characterization. Panel quality is assessed using ultrasonic c-scan and optical microscopy. Subsequently, tensile and flexural tests are conducted and the results compared with commercially available strand-based compounds. Finally, a brief analysis of cost-volume factors and global analysis of the environmental impact of upcycling TET is presented using the carbon dioxide equivalent (CO_2 eq) as a metric.

2. Materials and methodology

2.1. Materials

The TET strand material is a biproduct of Teijin's Tenax®-E TPUD PEEK-HTS45 P12 12 K-UD-145 unidirectional prepreg production line. The virgin tape itself, henceforth referred to as TPUD PEEK-HTS45, consists of standard modulus Tenax®-E HTS45 carbon fibre arranged in 12 K tows and impregnated with a PEEK matrix. The prepreg's areal weight and matrix content by weight are specified as 220 g m^{-2} and 34 %, respectively [10]. However, it is worth noting that TET strands recovered from this prepreg line are waste offcuts which may not meet the virgin material specifications. Lastly, square strands cut from the virgin TPUD PEEK-HTS45 prepreg and measuring 12.7 mm by 12.7 mm are used as a benchmark to compare against the results obtained from the TET strands.

2.2. Geometric characterization of as-received TET waste

A geometric characterization method is developed based on image analysis in order to measure the size and shape of TET strands before and after sorting. Photographs of the TET strands are taken against a white background (Fig. 2a). The images collected are post-processed using an image analysis code written in Python. The code performs the following steps to obtain information regarding strand geometry: 1. Image displayed and user prompted to define image scale using visible physical reference; 2. User prompted to crop imported image so that only strands are visible; 3. Image thresholding using Otsu's method; 4. Object (strand) detection and identification number designation; 5. Polygon best fit on all objects; 6. Identification of each polygon's two parallel sides and use as strand fibre direction; 7. Strand length, length distribution, width and area calculation; 8. Export collected data in.csv format. Note that the use of a strand's parallel edges to determine the fibre direction was manually validated on a large number of strands initially. Other methods were also considered, such as measuring the grayscale gradient vector across the strand surface, however the parallel edge method was found to be most reliable.

The length, width and aspect ratio distributions of 1503 as-received TET strands obtained through this image analysis are presented graphically in Fig. 3 as a box and whisker plot. In this figure, and throughout this work, the length is always associated to the fibre direction. Table 1 summarizes key elements from each distribution such as the mean, median, interquartile range (IQR), minimum and maximum values. The minimum and maximum whiskers are defined by the first data point present within the outlier bound of quartile 1 minus 1.5*IQR and quartile 3 plus 1.5*IQR, respectively. The strands measured feature very similar length and width distributions; however, most of the strands are either longer in the fibre direction, or very nearly square. This is supported by the data found within the lower and maximum quartiles, which represent 75 % of all the data, having aspect ratios of 0.91 – 2.23. IQRs of 8.4 mm – 27.3 mm for strand length and 8.0 mm – 23.4 mm for strand width provide baselines for the dispersion of each parameter, which can be compared with data collected from batches of sieved strands in later sections.

2.3. Strand sorting

2.3.1. In-plane circular motion sieving

A first attempt is made at sorting TET strands using a Model B Ro-Tap® sieve shaker from Tyler Industrial Products, which uses an in-plane circular motion to agitate its contents (Fig. 4). The sieve shaker is equipped with six U.S. standard sieves which measure 200 mm in diameter and 50 mm in height. Each sieve features a steel wire mesh (square) and are stacked such that the mesh cell size is progressively finer as follows: 28 mm, 20 mm, 14 mm, 10 mm, 5 mm and 2.5 mm.

Trials are carried out to determine the effect of sieving time and batch mass on sorting effectiveness according to the test plan shown in Table 2. The batch masses of 30 g and 100 g represent the quantities of strands needed to (1) simply cover the 28 mm sieve surface and (2) completely fill the 28 mm sieve. A total of three repetitions are carried out for each of the specified testing configurations.

For each test, batches of TET strands are prepared as follows: first, a large quantity of strands is spread over a working surface as shown in Fig. 4a; next, smaller quantities are taken from different locations at random to avoid preferential selection and placed in a steel bowl to be weighed using a digital scale; lastly, the strands are placed in the coarsest sieve at the top of the stack and loaded into the shaker shown in Fig. 4b. Following each trial, strands are collected from each sieve and weighed.

2.3.2. Linear vertical motion sieving

An alternative sorting approach using a TS-1 Gilson testing screen from Gilson Company, Inc. (Fig. 5) is explored. The TS-1 system features

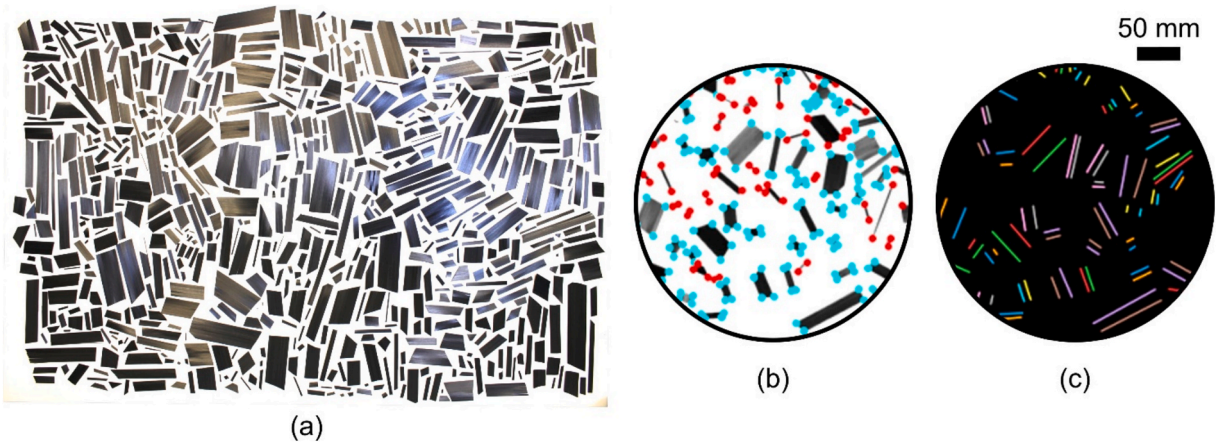

Fig. 2. (a) As-received strands photographed against a white background; (b) and (c) visual output of the image analysis Python code including thresholding, polygon fitting, and parallel line detection.

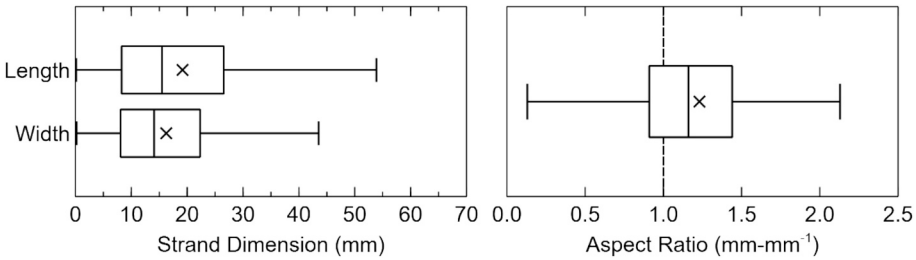

Fig. 3. Box and whisker plots showing the distribution of (a) strand length and width; and (b) strand aspect ratio.

Table 1
Key elements taken from the distributions shown in Fig. 3.

	Mean, "x"	Median, "|"	IQR (50 %)	Min	Max
Length	19.2 mm	15.5 mm	8.3 – 26.6 mm	0.1 mm	53.8 mm
Width	16.3 mm	14.1 mm	8.0 – 22.3 mm	0.2 mm	43.5 mm
Aspect Ratio	1.23	1.16	0.91 – 1.44	0.11	2.13

sieves measuring 451 mm × 667 mm × 67 mm and, unlike the Model B Ro-Tap®, uses a linear vertical motion to agitate its contents. The sieve stacking sequence (28 mm, 20 mm, 14 mm, 10 mm, 5 mm, 2.5 mm) is the same as in the circular motion sieving trials.

The batch preparation procedure for the TS-1 Gilson testing screen is kept the same as for the in-plane circular motion sieving trials. Given the greater size of the TS1 and the limited supply of TET material, batches of 1000 g and a single sieving time of 10 min are tested. A total of 14 such trials are carried out and the subsequent materials weighed.

2.4. Panel fabrication

Panels are compression moulded using a 305 mm × 305 mm invar picture frame tool and a 567 g strand charge. Strands are spread within the tool in small batches to ensure an even distribution and minimize out-of-plane strand orientation. Panel processing features a consolidation dwell of 30 min at 400 °C, a consolidation pressure of 1 MPa, and a slow cooldown at approximately 3–5 °C-min^{-1}. Material flash is trimmed from the panel edges following compression moulding, resulting in 278 mm square panels. Final panel thickness varies from 2.6 mm to 3.8 mm due to inconsistent amounts of flashing generated.

The panels made using the TET strands are named after the sieve

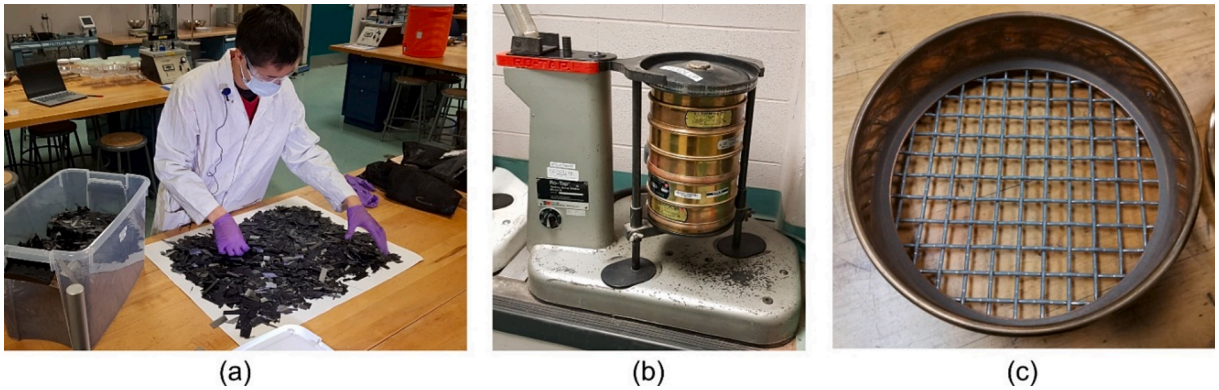

Fig. 4. (a) TET strands being spread over working surface prior to weighing; (b) model B Ro-Tap® sieve shaker with sieve stack installed; (c) U.S. standard wire mesh sieve.

Table 2
Experimental test plan designed to study the effect of sieving time and batch mass on sorting effectiveness.

	Configuration 1	Configuration 2
Batch Mass	100 g	30 g
Sieving Time	7, 10, 13 min	7, 10, 13 min
Repetitions	3	3

from which the strands were retrieved. As one or two panels are moulded in each case, the number 1 or 2 is added to the name to differentiate them. For instance, sorted 10 mm – 2 refers to the second panel made with strands retrieved from the 10 mm sieve. To have a better representation of the fibre length in a sieve and to understand its influence on mechanical properties, each TET strand analyzed is virtually divided into 2 mm wide strips along its length (see section 3.1). The average fibre length of the strands recovered in one sieve is then calculated by averaging the length of each strip. Table 3 below summarizes the different panels manufactured.

2.5. Panel characterization

2.5.1. Ultrasonic inspection

Each panel is scanned using TecScan's TCIS-1000 immersion ultrasonic inspection system and a Panametrics V309 probe with a diameter of 12.7 mm and a focal length of 50.8 mm. A frequency of 5 MHz is chosen [11,12] and data acquisition is carried out in steps of 1 mm, moving the probe along the panel at a speed of 12.5 mm/s. As the scan is unidirectional, the probe returns to the starting point after each pass and then shifts by 1 mm along the panel's other axis. The data collected is analysed using the TecView UT2 software.

2.5.2. Optical microscopy

Panels baseline – 2, sorted 2.5 mm and sorted 14 mm – 2 are selected for microscopic analysis, as they are made using strand batches with significantly different characteristics: namely, unsorted, smallest and largest strands, respectively. Specimen location is determined by overlaying the cutting plan of the mechanical testing specimens with the C-scan amplitude map, as will be shown later in Fig. 16. For each panel, microscopy specimens are taken from the following areas:

- C-scan peak amplitude greater than 80 %, referred to as *High Peak Amplitude*;
- C-scan peak amplitude between 35 % and 65 %, referred to as *Medium Peak Amplitude*;
- C-scan peak amplitude less than 20 %, referred to as *Low Peak Amplitude*.

Specimens are cut using a Dremel rotating saw tool and mounted in acrylic resin. They are polished using a MotoPol 2000 automatic grinder/polisher. They are then imaged using an Olympus GX51 optical microscope. Finally, multiple images are stitched together using GIMP image analysis software to obtain specimen mosaics.

2.5.3. Tensile tests

Tensile tests are conducted according to ASTM D3039, with seven specimens measuring 250 mm by 25 mm tested per panel. A ProtoMax waterjet cutting machine is used to cut specimens, which are then lightly polished to achieve straight edges. Tests are conducted at a displacement rate of 2 mm-min^{-1} with displacement measured via digital image correlation (DIC). Images are captured at a rate of 1 Hz using a single FLIR Grasshopper 3-51SM5M monochrome camera. Data is processed using the digital image correlation engine (DICe) software with a subset size of 35 pixels and a step size of 15 pixels. Strain is calculated as the average strain of each subset within an image using a Python program. The ultimate tensile stress is calculated as the maximum force applied divided by the cross-sectional area. Young's modulus is determined as the linear slope of the stress–strain curve between $\varepsilon = 0.1\%$ and $\varepsilon = 0.3\%$.

2.5.4. Flexural tests

Three-point bending flexural tests are conducted according to ASTM D790, with six specimens measuring 130 mm by 13 mm (32:1 span-to-depth) tested per panel. The maximum flexural stress and tangent modulus of elasticity are calculated following the guidelines put forth in the standard.

Table 3
Panels characteristics.

Panel name	Type of strands	Average fibre length	Quantity
Baseline	Unsorted TET	26.7 ± 17.1 mm	2
Sorted 2.5 mm	2.5 mm sieve	15.8 ± 11.2 mm	1
Sorted 5 mm	5 mm sieve	20.9 ± 12 mm	2
Sorted 10 mm	10 mm sieve	22.8 ± 10.8 mm	2
Sorted 14 mm	14 mm sieve	34.1 ± 15.3 mm	2
Virgin	Square strands	12.7 mm	1

Fig. 5. (a) TS-1 Gilson testing screen; (b) and (c) examples of the Gilson sieves with and without TET strands, respectively.

3. Results and discussion

3.1. Strand sorting

3.1.1. In-plane circular motion sieving

The TET strand masses recorded following each trial (Fig. 6) show the quantity of strands recovered from the top two to three sieves (28 mm, 20 mm, 14 mm) decreases with increasing sieving time, while the quantity of strands recovered from the bottom two to three sieves (5 mm, 2.5 mm, Bottom) increases. This result suggests that neither 7 nor 10 min is sufficient time for strands to complete their journey through the sieve shaker. A convergence between the 30 g and 100 g batches is observed after 13-minutes with both distributions looking quite similar. Most of the TET strands were found to have settled in the 5 mm – 14 mm sieves after 13 min, with 74 % settling there for the 30 g batches and 67 % settling there for the 100 g batches. It seems likely that the mass distribution of the 100 g batches would have continued to evolve given longer sieving times; however, there was evidence of strand damage (e.g., splitting, breakage) after 13 min which may represent a limiting factor for this type of sieving method.

After many of the initial sieving trials, strands were found to have clumped together into aggregates in the top three sieves. Examples of these aggregates are shown in Fig. 7. A visual inspection revealed that many smaller strands had become trapped within these aggregates, thus limiting their ability to pass into the finer sieves.

A second test campaign (Table 4) was carried out to study the effect of increasing batch mass (*i.e.,* sieve crowding) on aggregate formation for a fixed sieving time of 13 min. Aggregates were collected from the 28 mm, 20 mm, and 14 mm sieves after each test and weighed. Each aggregate was then deconstructed and the resulting strands analyzed according to the method from section 2.2. The quantity of strands that should have passed down to finer sieves was determined by comparing the mesh cell size to each strand's smallest dimension. Strand area was then used to quantify the amount of out-of-place strands, as it is equivalent to strand mass assuming a somewhat consistent prepreg areal weight.

The mass of aggregates recovered from each of the top three sieves relative to the batch mass is shown in Fig. 8a. Similarly sized aggregates were consistently formed for batch masses of 10 g, 20 g, and 30 g with the mass distribution showing similarities to the 13-minute-long trials presented in Fig. 6. The size of aggregates found in the 28 mm sieve increased noticeably for the 100 g batch mass, suggesting that strand overcrowding may be principally responsible for the formation of aggregates. This is further supported by the fact that aggregate sizes in the 14 mm sieve decreased by roughly 50 % when only 5 g was used.

Fig. 8b shows that a significant amount of strands that are small enough to pass into finer sieves remain caught inside of aggregates. This phenomenon increases, as one would expect, with batch mass and hinders the effectiveness and practical implementation of this sorting method.

3.1.2. Linear vertical motion sieving

Unlike in the in-plane circular motion trials, no aggregates were found in any of the 14 batches processed using the TS-1 linear vertical motion system. Fig. 9 compares the masses of recovered TET strands from one representative TS-1 trial with those from both 30 g and 100 g circular motion trials in which sieving time was also 10 min.

Two key differences stand out. Firstly, little material remains in the 28 mm and 20 mm sieves after the linear vertical trials (4.8 % cumulative), compared to as much as 22.0 % (30 g) and 26.1 % (100 g) after the in-plane circular trials. Secondly, more than half of the strands are found between the 14 mm and 5 mm sieves (69.6 % cumulative) with the TS-1, while the in-plane circular method resulted in a more homogeneous distribution.

It was possible to operate the Gilson TS-1 system without its enclosing panels. A Chronos 2.1-HD high speed camera from Kron Technologies was used to record the 28 mm sieve during one of the sieving trials (Videos 1, 2 and 3) at a frame rate of 1000 fps. Fig. 10 shows still frames captured at the beginning of the trial (Fig. 10a), after 2 min (Fig. 10b) and after 4 min (Fig. 10c), respectively. These recordings show that the 28 mm sieve is essentially emptied after as little as 4 min, while anywhere from 10 – 20 % of strands remain in the 28 mm sieve following circular motion trials that lasted 7 – 13 min and where the sieve shaker was similarly loaded (*i.e.,* 100 g, Fig. 6). This result, along with the absence of aggregates, informed the authors' decision to move forward with a focus exclusively on the linear vertical motion sieving solution.

Identifying which strand characteristics influence their passage through the Gilson TS-1 sieving system should provide insight into the type of strands to be found in each sieve following sorting. This information should ultimately help guide the selection and optimization of the sieve stacking sequence, based on initial TET characteristics. Strands recovered from the Gilson sieves were imaged and analyzed using the python code described in section 2.2. The resulting distributions for average strand length, width, area and minimum dimension are presented in Fig. 11, along with the corresponding sieve cell sizes shown in translucent cyan. Cell size is represented here as either a range or an area. The former is defined as the square cell side length to the cell diagonal dimension. In the case of the 10 mm sieve, the cell size is therefore given as 10 mm in lateral length to 14 mm in diagonal length, with a cell surface area of 100 mm^2. Table 5 presents results by comparing only the distribution averages, excluding strand area, to the cell size of the sieve the strands were last able to pass through (*i.e.,* upper sieve, or previous sieve).

The data presented suggest that the TET strands have been separated by size through sieving, as evidenced by the consistent decrease in average geometric characteristics with decreasing sieve cell size. An exception is observed with the width and minimum dimension of strands

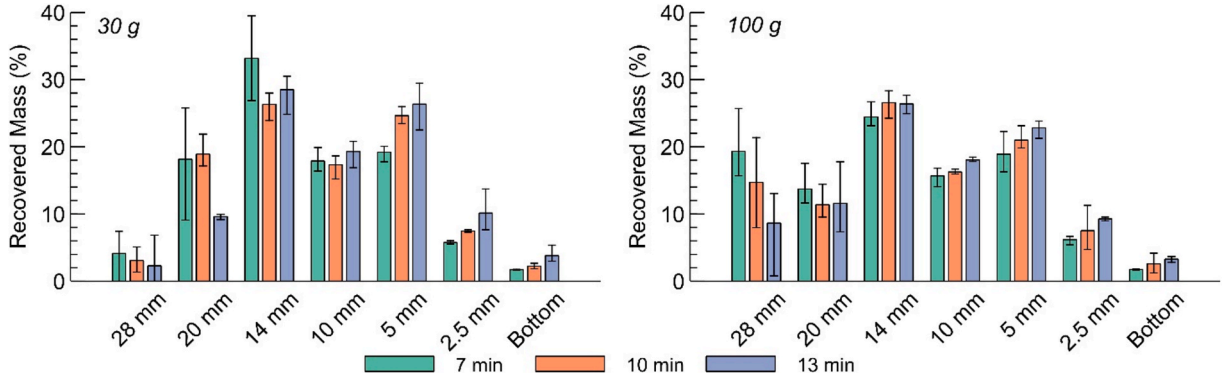

Fig. 6. Mass distributions of recovered TET strands organized by batch mass for the in-plane circular motion shaker after various sieving times.

Fig. 7. TET strand aggregates found in a number of different sieves following circular sieving trials.

Table 4
Aggregate formation test plan.

Batch Mass	5, 10, 20, 30, 100 g
Sieving Time	13 min
Repetitions	5

found in the 28 mm sieve, which are noticeably smaller than those of strands found in the subsequent 20 mm and 14 mm sieves. This appears to have been caused by the partial splitting of certain strands, resulting in them being caught on the mesh wire (Fig. 12b). There were also some strands found in the 28 mm sieve which featured long slender protrusions which likely prevented them from passing through the mesh (Fig. 12a).

Comparing the geometric characteristic distributions of strands from a given sieve with the cell size of the sieve immediately above (*i.e.,* the sieve last passed through) reveals that the minimum dimension of the strand, which more often than not corresponds to the strand width, is responsible for governing the movement of strands through the system. Assuming the strands do not undergo significant bending or twisting during sieving, a strand found in the 10 mm sieve last passed through the 14 mm sieve, which has a cell size range of 14 mm – 20 mm and a cell area of 196 mm^2. Considering:

- With an average length of 23.09 mm, the strand cannot pass lengthwise through the 14 mm sieve.
- With an average area of 332.54 mm^2, it cannot pass flatwise.
- With an average width of 13.84 mm, it can pass by aligning itself widthwise with the mesh.

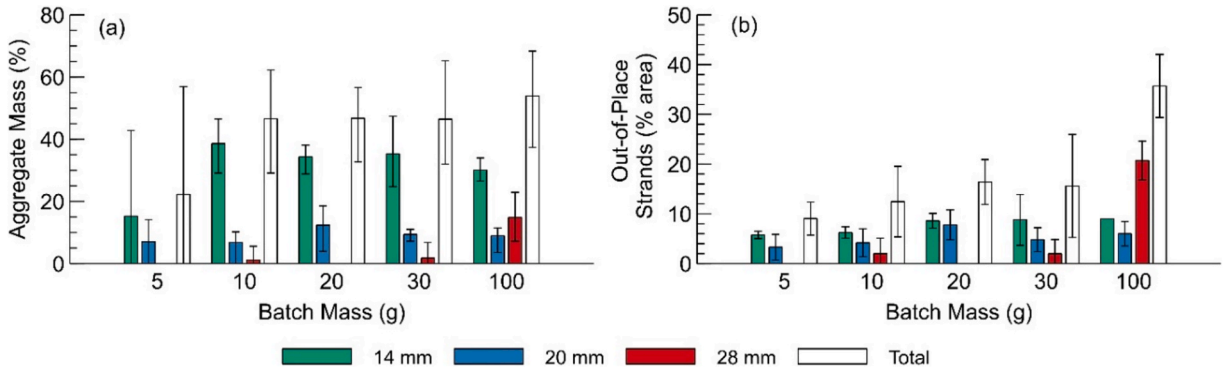

Fig. 8. (a) Percent mass of aggregates and (b) percent area of out-of-place strands found in the top three sieves for the in-plane circular motion shaker.

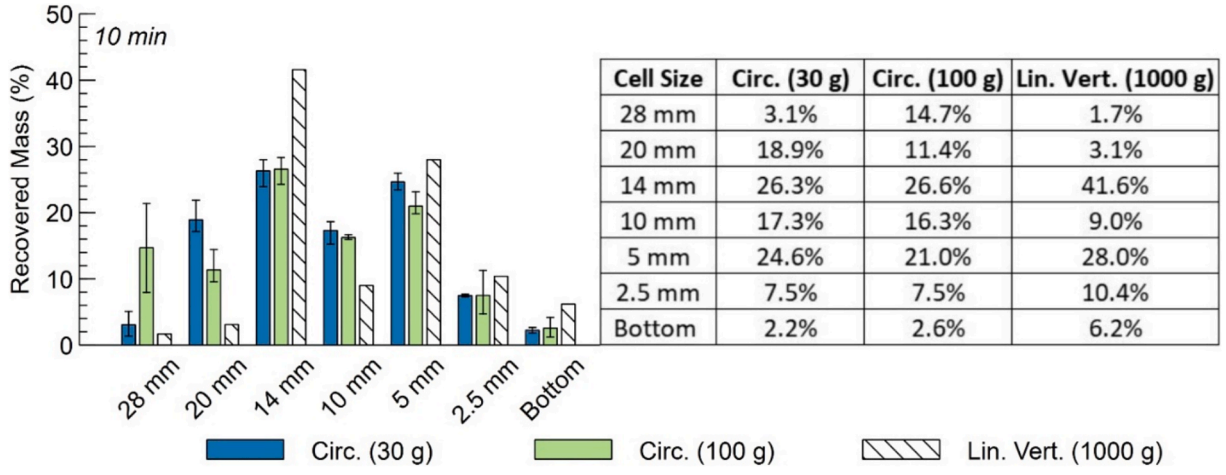

Cell Size	Circ. (30 g)	Circ. (100 g)	Lin. Vert. (1000 g)
28 mm	3.1%	14.7%	1.7%
20 mm	18.9%	11.4%	3.1%
14 mm	26.3%	26.6%	41.6%
10 mm	17.3%	16.3%	9.0%
5 mm	24.6%	21.0%	28.0%
2.5 mm	7.5%	7.5%	10.4%
Bottom	2.2%	2.6%	6.2%

Fig. 9. Mass distributions of recovered TET strands from both in-plane circular and linear-vertical motion sieving.

Fig. 10. Distribution of strands in the 28 mm sieve at (a) 0 min; (b) 2 min and (c) 4 min of sieving time.

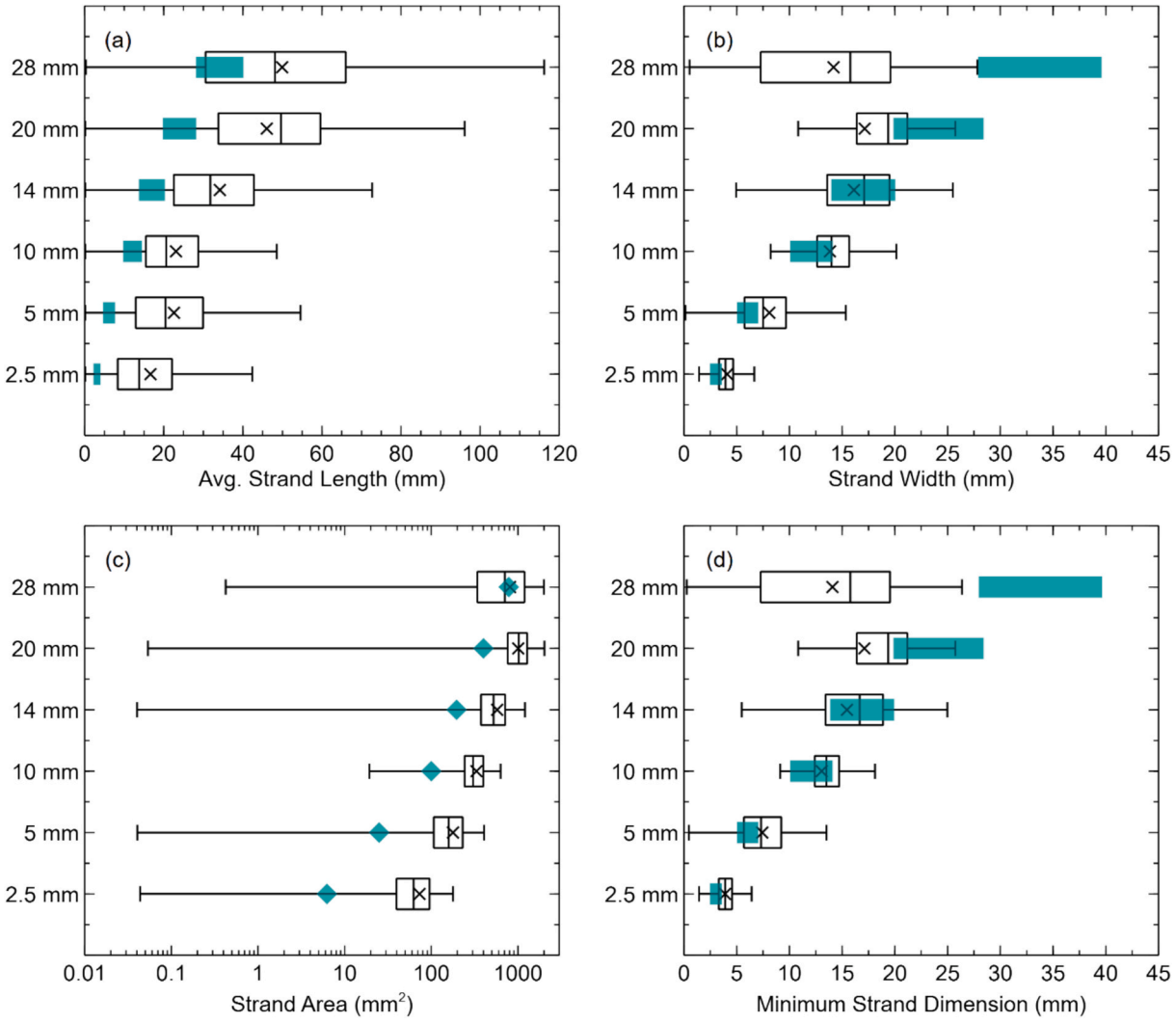

Fig. 11. Strand geometric characteristic distributions obtained from image analysis of strands passed through the Gilson TS-1 sieve shaker for 10 min and 1000 g batch. Cyan bars represent the cell sizes defined by the square cell side length, diagonal length and area. Cyan diamond markers represent cell area.

Table 5
Average values taken for recovered strands. n represents the number of strands used to calculate the average values.

Sieve	28 mm (n = 170)	20 mm (n = 215)	14 mm (n = 306)	10 mm (n = 528)	5 mm (n = 966)	2.5 mm (n = 2686)
Mesh Size of Previous Sieve	–	28 – 40 mm	20 – 28 mm	14 – 20 mm	10 – 14 mm	5 – 7 mm
Strand Avg. Length	49.92	46.04	34.17	23.09	22.56	16.63
Strand Avg. Width	14.18	17.14	16.11	13.84	8.09	4.10
Strand Avg. Min. Dim.	14.08	17.11	15.46	13.06	7.43	3.90

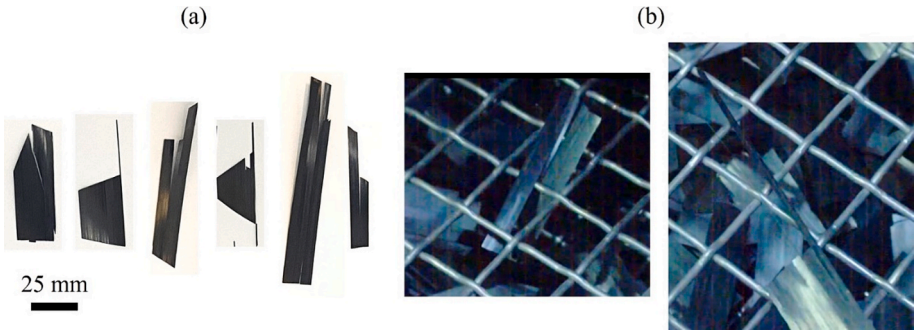

Fig. 12. (a) Strands from the 28 mm sieve with some presenting damage caused by the mesh wire; (b) Example of a strand trapped in the mesh wire preventing it from passing through the lower sieve.

The majority of these strands have greater lengths and areas than the sieve immediately above, while the opposite is true of strand widths, which are consistently smaller than or equal to the cell size of the sieve immediately above. However, the box plot in Fig. 3b shows that there is a proportion of unsorted strands that are wider than they are long. Fig. 13 illustrates the two shapes of strands corresponding to an aspect ratio greater or less than 1, where the length is defined by the orientation of the fibres. Therefore, in the case of a strand with a width greater than its length, the passage through the sieves is determined by the length. It is thus more appropriate to consider the minimum dimension as the parameter governing the passage of the strands during sieving.

Up until this point, the length of each strand has been calculated by averaging its sides which are aligned with the fibre direction. While this method is sufficient for quantifiably tracking strand sorting as objects, it is not appropriate for representing the length of fibres found in compression moulded panels made from strands as they flow and decompose. Instead, strands were virtually segmented using the images collected into 2 mm-wide strips and a global batch average based on the length of each strip was calculated. Fig. 14a shows this new method, applied to both baseline and sieved TET batches, highlighting the notable increase in the average fibre length as a function of sieve size. Images of each batch are also included in Fig. 15 to provide the reader with a corresponding visual reference. Fig. 14b presents the average fibre length and fibre length variation for each sieved batch relative to the baseline values. Sieving has produced batches with average fibre lengths that are both shorter (2.5 mm – 10 mm sieves) and longer (14 mm – 28 mm sieves) than the as-received TET waste. Furthermore, all batches except 2.5 mm exhibit significantly lower strand length variation compared to the baseline. The 14 mm batch is of particular interest, as it constitutes 41.6 % of the material recovered after sieving, has an average fibre length 7.39 mm longer than the baseline, and a fibre length variation 19.3 % smaller.

3.2. Panel quality

3.2.1. C-scan analysis

A colour scale is used to represent the C-scan echo amplitude, with more significant discontinuities shown as more blue and less significant discontinuities shown as more red. The TET-strand panels feature a highly heterogeneous *meso*-structure. This can be attributed to the disordered initial strand orientation distribution within the mould, the diversity of strand size and shape, and the processing-induced flow-compaction deformation.

During preliminary ultrasonic inspections, certain background echoes became saturated which reduced C-scan quality, thereby making it difficult to distinguish between noise and areas of potential defects. A threshold of 80 % peak amplitude was implemented to address this limitation, which is an approach for panels made of commercially available virgin strands [11,13].

Fig. 16 shows C-scans of the three panels that were also selected for microscopy analysis. Overlayed on each image is the cutting pattern used to extract optical microscopy specimens and mechanical test coupons. Generally speaking, the baseline-2 (unsorted) and sorted 2.5 mm – 1 show uniform panel structure with a very small number of discontinuities detected within the mechanical test coupons. The C-scan obtained for the sorted 14 mm – 2 panel, however, shows a significant

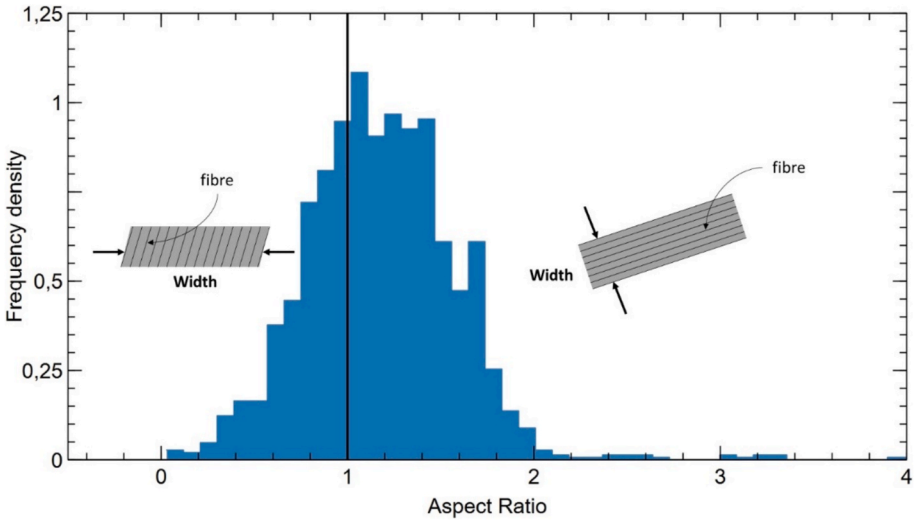

Fig. 13. Histogram of strand aspect ratio for recovered unsorted TET strand waste.

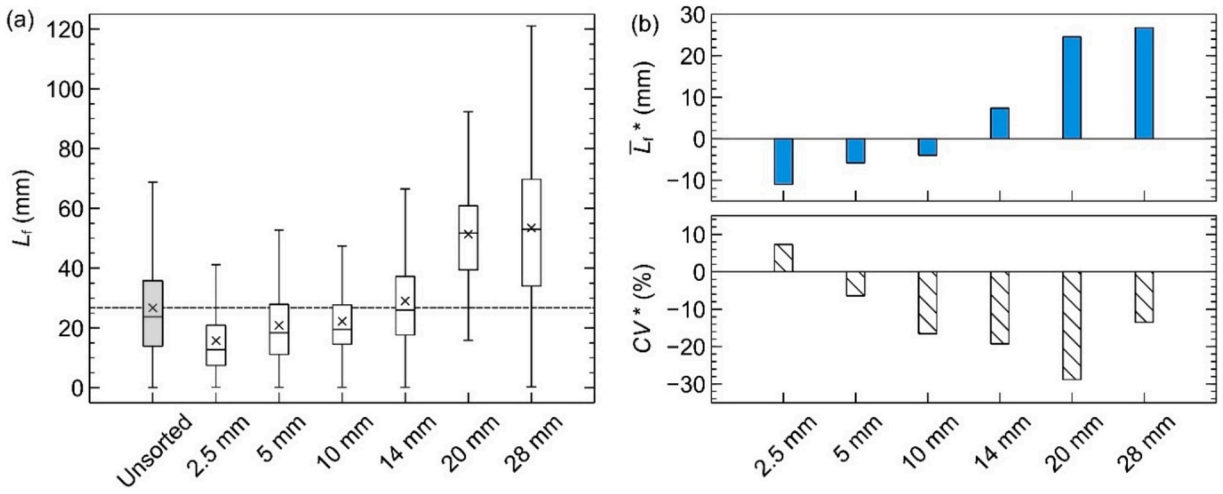

Fig. 14. (a) Evolution of strand fibre length using the 2 mm-wide strip method; (b) difference between average fibre length and coefficient of variation (CV) for each sieve compared with unsorted strands values.

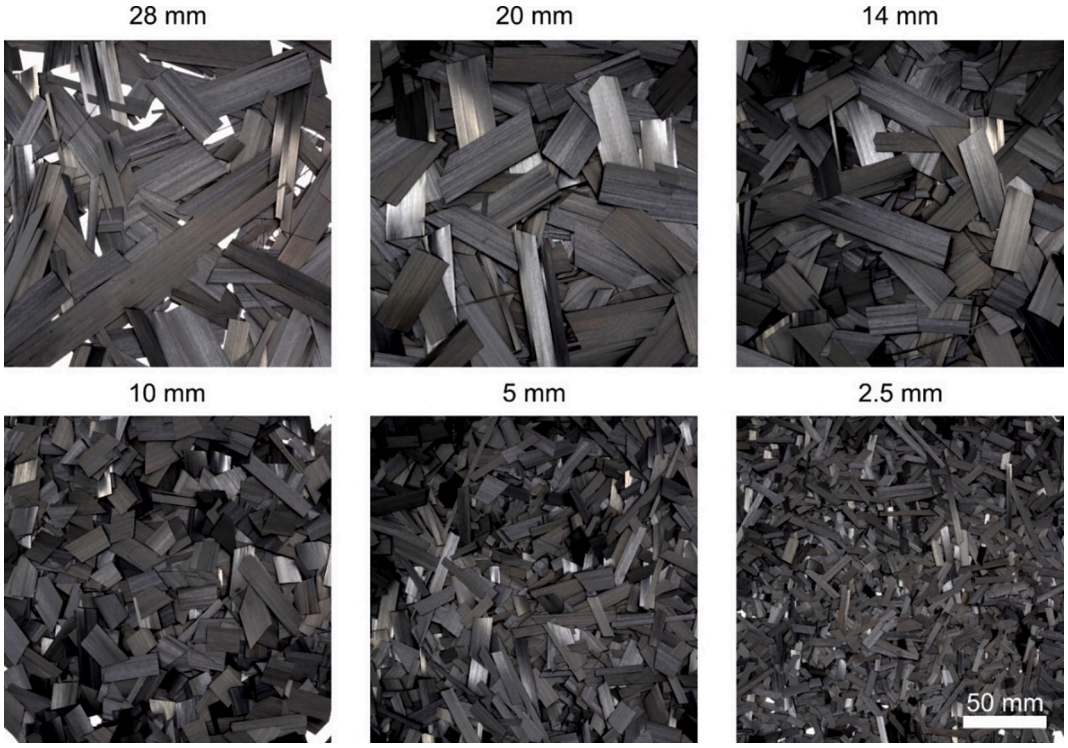

Fig. 15. Strands recovered in each sieve after sorting with the Gilson TS-1.

number of high-amplitude discontinuities running through the panel centre.

Different types of defects are revealed by analysing samples taken from hotspot areas (Fig. 17). Fig. 17c shows a line of porosity (black dot) observed in one sample. The corresponding portion of the c-scan for this same zone is characterized by several black pixels. When the wave passes through the piece and encounters a porosity, the echo produced is characterized by a large amplitude. Thus, just a few closely located porosities are enough to produce a black pixel, qualifying the region as a hotspot, even though the measured local porosity rate is low at 0.49 %. Porosities are also observed inside resin-rich pockets or scattered randomly within the specimen.

Other defects such as fibre swirls (Fig. 17a), out-of-plane orientation of the strands (Fig. 17b) and resin rich areas (Fig. 17b, c) are also found. Resin rich areas are more prevalent in sorted 2.5 mm panels compared to the other two panels, possibly due to the quantity of strands used. The TET retrieved from the 2.5 mm sieve are the smallest strands. The number of TET required to make one panel is therefore larger for the sorted 2.5 mm than for the other sieves. During compression moulding, the resin melts and fills the spaces between the strands, which are more common in the sorted 2.5 mm due to the higher number of strands used. Therefore, resin-rich regions are more likely to occur in panels manufactured using small strands.

In the second category, *i.e.*, the zones with peak amplitudes between 35 and 65 %, some defects are observed but in general they are smaller and less significant relative to the thickness of the sample. The last category, where the peak amplitude is lower than 20 %, is mostly free of defects, aside from small resin pockets at the ends of strands. The strands

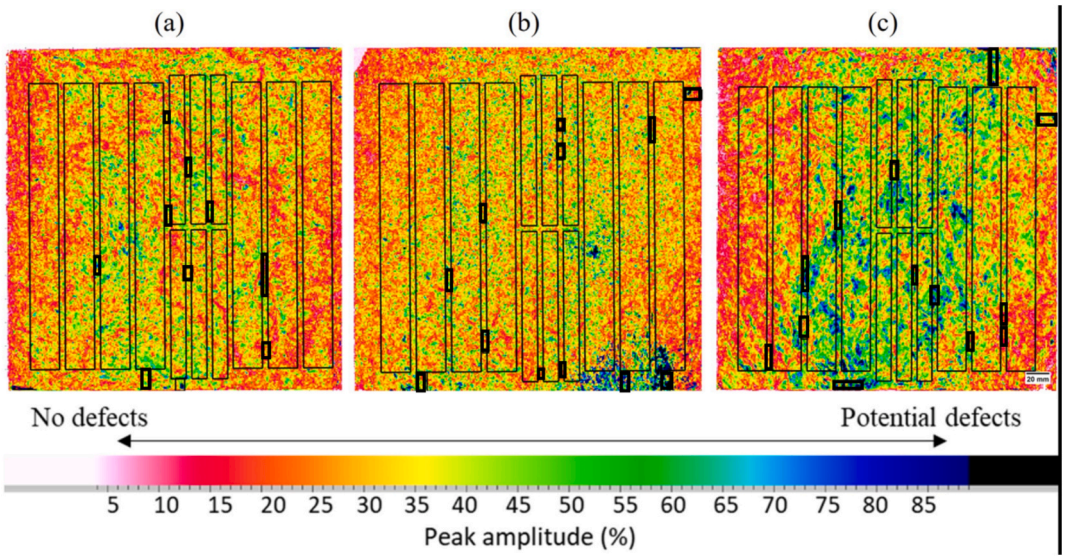

Fig. 16. Overlay of C-scan and cutting patterns of the samples for tensile, flexural and microscopy. (a) Baseline – 2 made with unsorted strands; (b) sorted 2.5 mm and (c) sorted 14 mm – 2.

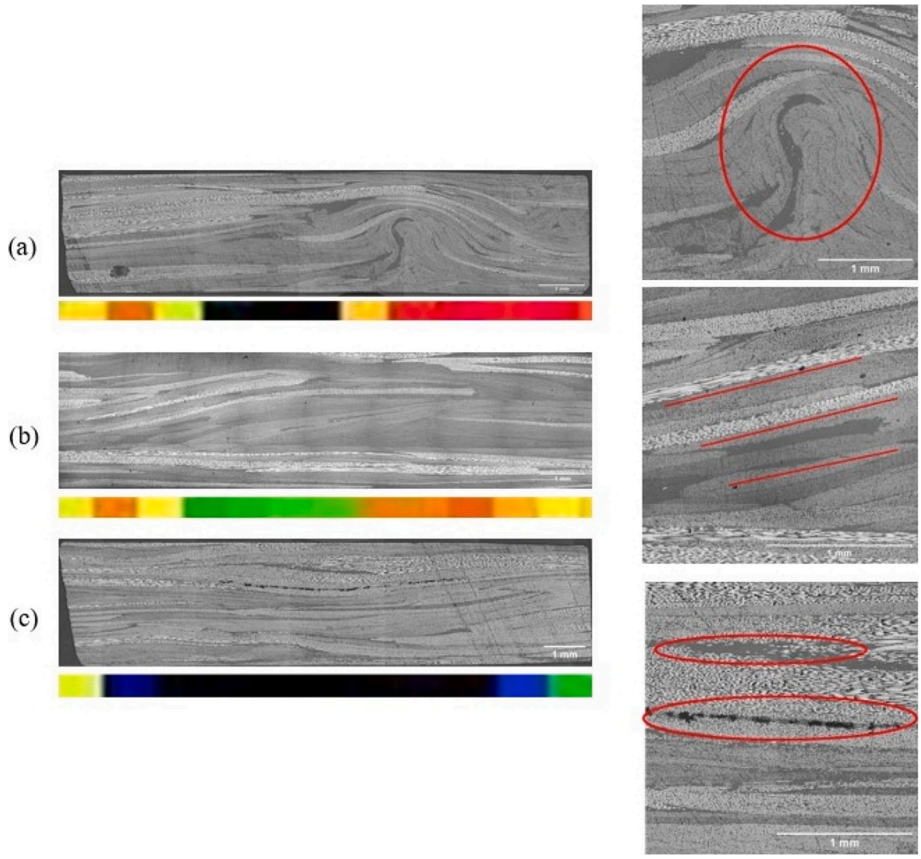

Fig. 17. Micrographic images of (a) fibre swirl with resin rich area; (b) strands oriented out-of-plane with some resin pockets; (c) line of resin at the top and line of porosity at the bottom. Microscopic images obtained on coupons extracted from a panel compression-moulded using strands retrieved from the 2.5 mm sieve.

are well stacked one on top of another and oriented in plane.

Ultrasonic analysis coupled with microscopy allowed the assessment of the quality of the panels, leading to several conclusions. First, the defects associated with the use of recycled TET strands are similar to those observed in commercial products. These defects include resin-rich regions, porosities, fibre swirling, and out-of-plane strand orientation, each of which can be observed alone or in combination with others. In the absence of hotspots, the measured void content (calculated by ImageJ software as the ratio between the porosity area and the image area) does not exceed 0.2 %, and areas with low amplitude echoes exhibit well-stacked strands with few resin-rich regions. Finally, hot-spots, or regions where peak amplitudes exceed 80 %, reveal at least one of the following features: clusters of porosities or large defects relative to the thickness of the samples. Therefore, ultrasonic inspection effectively

provides an indication of the presence or absence of defects.

3.3. Mechanical properties

3.3.1. Tensile properties

Measured tensile properties are shown relative to the corresponding panel fibre length in Fig. 18 (Tensile strength) and Fig. 19 (Young's modulus). The values displayed correspond to the property mean with standard deviations. Data found in the literature for panels made with similar strand-based composites are also presented for comparison purposes.

Tensile strength increases with increasing average fibre length. When comparing the smaller strands from the 2.5 mm sieve to the larger ones from the 14 mm sieve, a noticeable increase in strength is obtained as shown in Fig. 18. However, this is not the case for the tensile modulus. The average stiffness values obtained are relatively close from one to another and appear to be less affected by fibre length. Specimens made of TET retrieved from the 2.5 mm, 5 mm, and 10 mm sieves also present similar strengths, except for the Sorted 5 mm-1 panel which stands out with results equivalent to those of the Sorted 14 mm panels. Findings in the literature suggest that the use of larger strands favours greater overlap, thus lengthening the failure path and leading to higher strength values [5].

Data from the literature or provided in technical datasheets are used for comparison with the panels made here from TET strands. All values used for comparison come from compression-moulded panels with strand-based composites. The measurements from Eguémann [3], Kravchenko [14], and data from Toray (Cetex MC1200) [1] are for CF/PEEK strands, as in the current study. Commercial products are characterised by strands with fixed dimensions and a consistent fibre content, which is not the case with TET strands. The Sorted 14 mm – 1 & 2 and Sorted 5 mm – 2 stand out with values surpassing those of virgin products for both tensile strength and modulus. On average, panels made from TET strands exhibit more favourable strengths compared to virgin products with a fibre length of 12.7 mm. Despite corresponding to shorter fibre lengths, the data from Kravchenko [14] show an average modulus equal to or higher than those of the sorted 2.5 mm, sorted 5 mm – 1, and sorted 10 mm 1 & 2. Two-thirds of the panels have moduli lower than that of Cetex MC1200 [1].

All of the panels tested exhibit significant variation in both tensile strength and modulus. Even the most consistent panel, Sorted 5 mm – 1, features a 9.6 % CV for strength (357.3 MPa +/- 44.7 MPa) and a 5.6 % CV for modulus (44.7 GPa +/- 2.5 GPa), while the least consistent panel, Sorted 14 mm – 1, features a 50.0 % CV for strength (348.2 MPa +/- 174.3 MPa) and a 28.8 % CV for modulus (45.2 GPa +/- 13.0 GPa).

While sieving was shown to improve strand batch homogeneity in Fig. 14b, this effect has clearly not translated to more consistent tensile performance. As evidence, take again the Sorted 14 mm – 1 panel which has 19.4 % less variation in fibre length compared to the Baseline – 2 panel, but whose specimens exhibit significantly higher variation in tensile strength. Similarly, the Sorted 2.5 mm panel features 7.2 % more variation in fibre length compared to Baseline – 2, and yet its specimens are also less variable in terms of strength. Most telling perhaps, is that the panels manufactured from virgin strands, both here and in the literature, exhibit property variation on the same order of magnitude as the TET specimens, despite having essentially zero fibre length variability.

It must then be concluded that fibre length variability is not related to tensile property variability for strand based composite materials. This is supported by Fig. 20 which shows the coefficient of variation for both tensile strength and modulus plotted against the corresponding panel fibre length coefficient of variation. It is more likely that the stochastic nature of the strand orientation distribution within the mould and the further deformation caused by material flow during processing are responsible for the observed mechanical behaviour.

Analysis of the failure modes reveals a failure dominated by the matrix, in accordance with conclusions found in the literature for commercial strands. More than three-quarters of the samples break into two pieces. The most observed failure mode is the pulling out of strands, with little fibre breakage noted. Fig. 21 is a good example. The red arrows in the image show the strands that have pulled out on either side of the rupture zone.

The study of displacement using DIC allows for the comparison of the evolution of strain concentration areas with the hotspot areas of the C-scans. Fig. 22 highlights failure near a hotspot in the first column (a) and far from it in the second (b). The first row of the image is the C-scan of the tensile sample gauge. As a reminder, the hotspots correspond to the areas with blue pixels, and both specimens present one. The second row shows the strain field one second before the failure using DIC. In the first case, it can be observed that the strain concentration area is in the same region as the hotspot, while they are rather opposite in the second case. Finally, the last row shows the broken samples, confirming the interpretations of the first two rows. Even if the zones showing maximum deformation are sometimes linked to the hotspot area, only 26 % of samples break close to a hotspot. Therefore, it is not possible to conclude that failure is dominated by the hotspots.

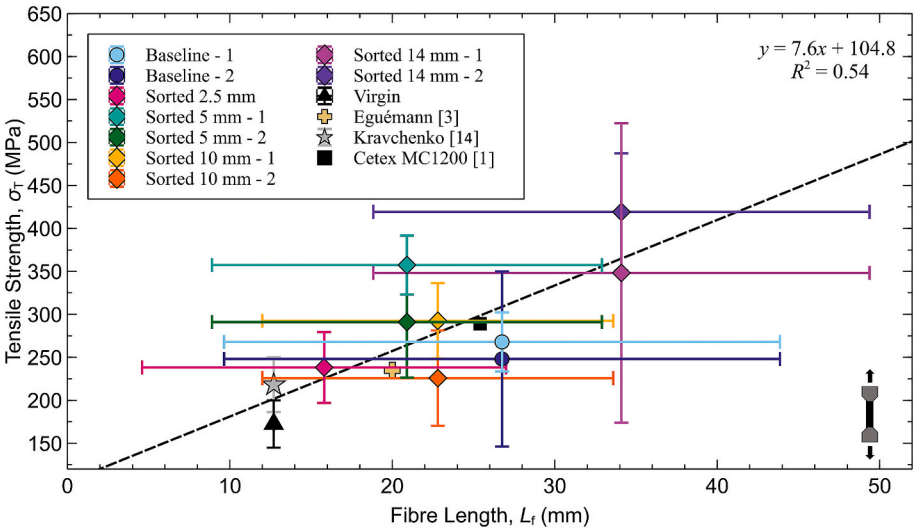

Fig. 18. Evolution of the tensile strength relative to the fibre length.

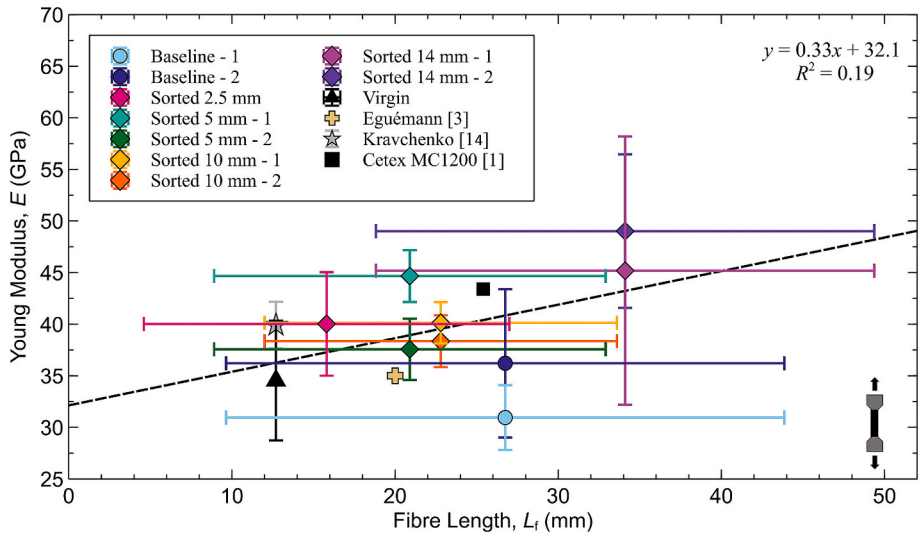

Fig. 19. Evolution of the Young Modulus relative to the fibre length.

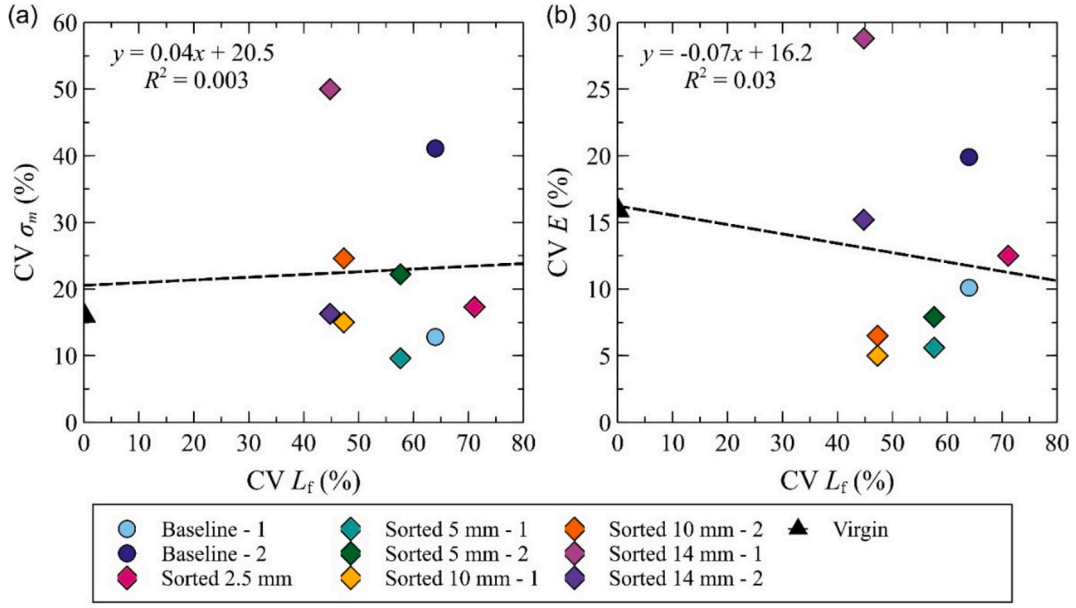

Fig. 20. Evolution of (a) the variation in tensile strength and (b) modulus, relative to the variation in fibre length.

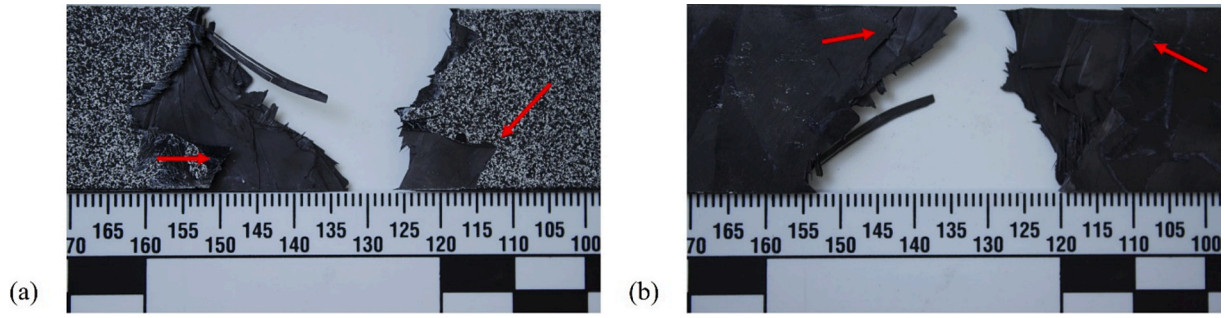

Fig. 21. Strand pulling out during the failure (a) front view and (b) back view.

3.3.2. *Flexural properties*

As with the tensile tests, the results of the flexural tests are shown in Fig. 23 and Fig. 24 for strength and modulus, respectively. Once again values from literature are used to compare TET strands with strand-based composites.

The trend of variability in results observed in the case of tensile testing persists for flexural testing, regardless of the type of strands. Fig. 23 highlights the improvement in average flexural strength as a

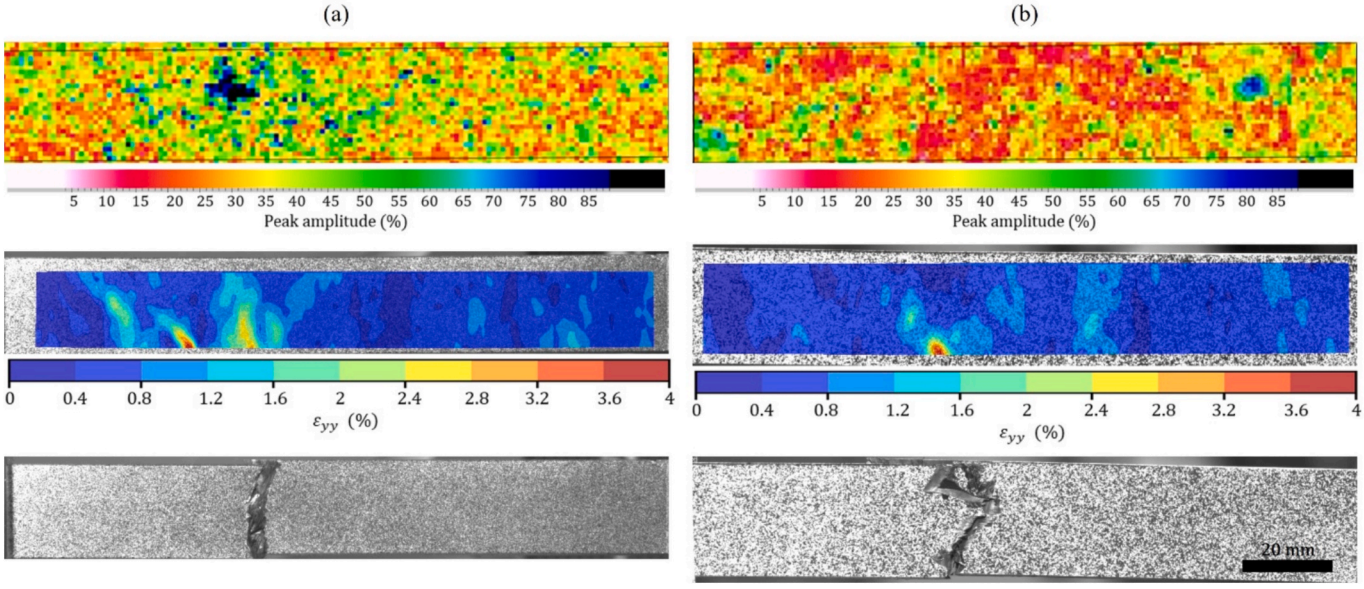

Fig. 22. Tensile sample C-scans, strain fields before failure and broken samples (a) near a hotspot and (b) far from a hotspot.

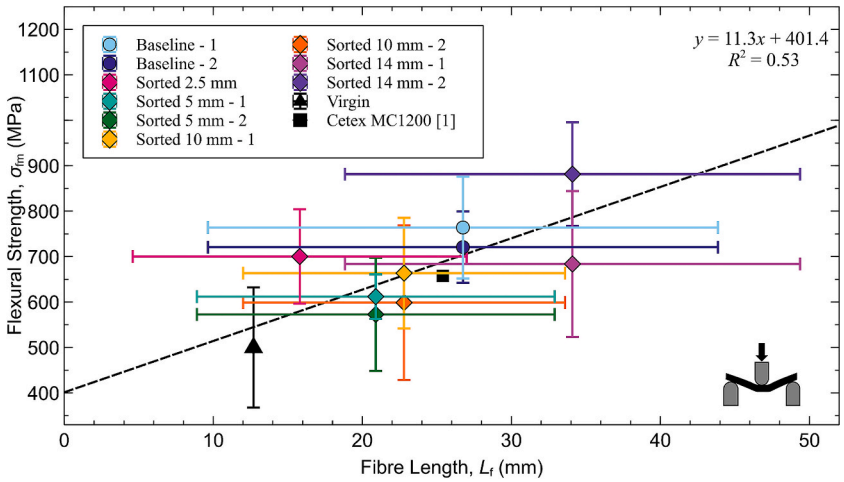

Fig. 23. Evolution of flexural strength relative to the fibre length.

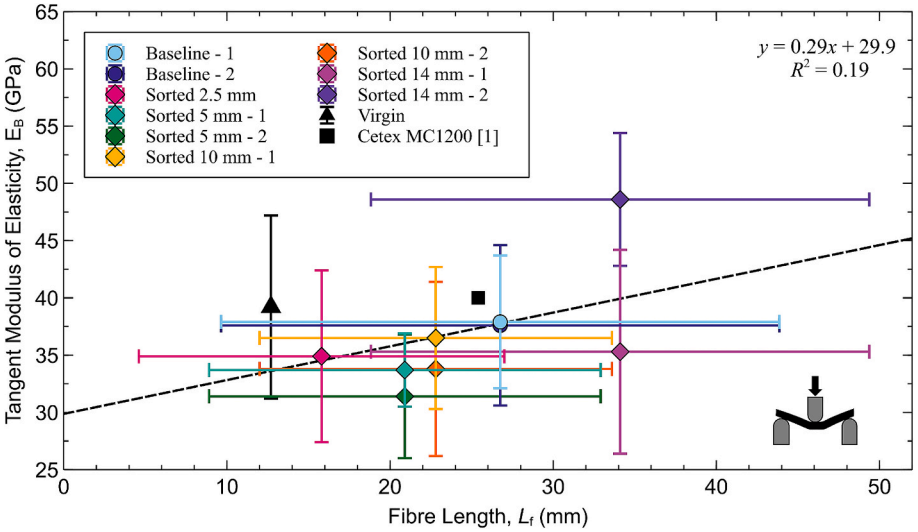

Fig. 24. Evolution of flexural tangent modulus relative to the fibre length.

function of fibre length for panels made from sorted TET strands, whereas the influence is not as present for the modulus. Flexural strengths are on average higher than tensile strengths. This fact had already been observed for fibreglass/epoxy strands [4].

By again comparing the coefficients of variation of the strengths and moduli with that of the fibre lengths (Fig. 25), it becomes clear that no specific pattern stands out. Thus, just as with tensile testing, the variability of the results cannot be attributed to the geometric variability of the strands. This reinforces the hypothesis of the role of the orientation of the strands within the samples.

Despite having the shortest fibre length, the sorted 2.5 mm panel exhibits superior properties compared to the panels from the 5 mm and 10 mm sieves. The performance of these panels is very similar, whether comparing specimens from the same sieve or between the two sieves. This could be explained by similar average fibre lengths. Concerning the baseline panels made with unsorted strands, they exhibit better average properties than the other sorted panels, except for the sorted 14 mm – 2, which again differentiates itself with the highest performance.

There is not as much data available for flexural tests as there is for tensile tests in the literature. Therefore, the comparison between recycled and commercial strands is made using the values obtained from tests on the virgin panel (12.7 mm square flakes) and the Cetex MC1200 [1] data sheet. The results of commercial products fall within the range of values for recycled products. Focusing on the average values and comparing them with those of the panels having the closest average fibre length, which is the 2.5 mm for virgin and the baselines for the Cetex MC1200 [1], it is observed that the moduli are higher than almost all the average values obtained for TET. As with the tensile tests, the use of recycled strands (sorted or unsorted) results in higher flexural average strengths than commercial products.

Based on the tensile and flexural results, sorting does not seem necessary in term of mechanical properties as the direct reuse of strands yields satisfactory results compared to commercial materials. However, the sieving process sorts the TET based on the fibre length and higher average tensile and flexural strengths are obtained for the TET strands recovered from the biggest sieve. Therefore, a decision to implement or not a sieving process prior to using the TET strands will depend on the desired mechanical properties but mostly, on the geometric features of the parts to be made. Indeed, the sieving process sorts the TET according to their size which influences the flow of the material. The TET recovered from the smallest sieves will better adapt to geometrically complex shapes than those recovered from the biggest sieves. In all cases, the inherent variability of strand-based composites remains.

4. Recycling potential

4.1. Scaling Considerations

The Teijin thermoplastic prepregging line from which the TET strands studied here were recovered is capable of producing rolls with widths (w_r) of either 304.8 mm or 609.6 mm. Using the results of the geometric characterization described in Section 2.2, the prepreg scrap rate can be estimated using Eq. (1).

$$ScrapRate = (2{*}w_s{*}100)/w_r \quad (1)$$

Table 6 presents the results obtained for the two roll widths. To have a representative estimate of the actual scrap rate, three scrap rates are calculated using the IQR bounds and the average width of the TET strands (w_s)

In an article edited by CompositeWorld [15], it is stated that the Heinsberg prepregging line has a maximum production capacity of 320,000 kg per year for the 609.6 mm wide rolls. No annual production capacity is specified for the smaller roll width and the following calculations are thus based the larger 609.6 mm wide roll. Having determined the scrap rates for this roll width, it is possible to calculate the annual TET waste mass generation. Using a similar approach to the previous calculation and assuming an unknown line usage rate, the waste mass is calculated for 20 %, 40 %, 60 %, and 80 % of line usage. All these quantities are summarized in Table 7, using the medium scrap rate from Table 6 (5.3 %).

In one year, TET strands waste production generated by one

Table 6
Scrap Rate estimation for two roll widths.

	Scrap Rate		
Roll Width (w_r)	Low (w_s = 8 mm)	Medium (w_s = 16.3 mm)	High (w_s = 22.3 mm)
304.8 mm (12 in)	5.2 %	10.7 %	14.6 %
609.6 mm (24 in)	2.6 %	5.3 %	7.3 %

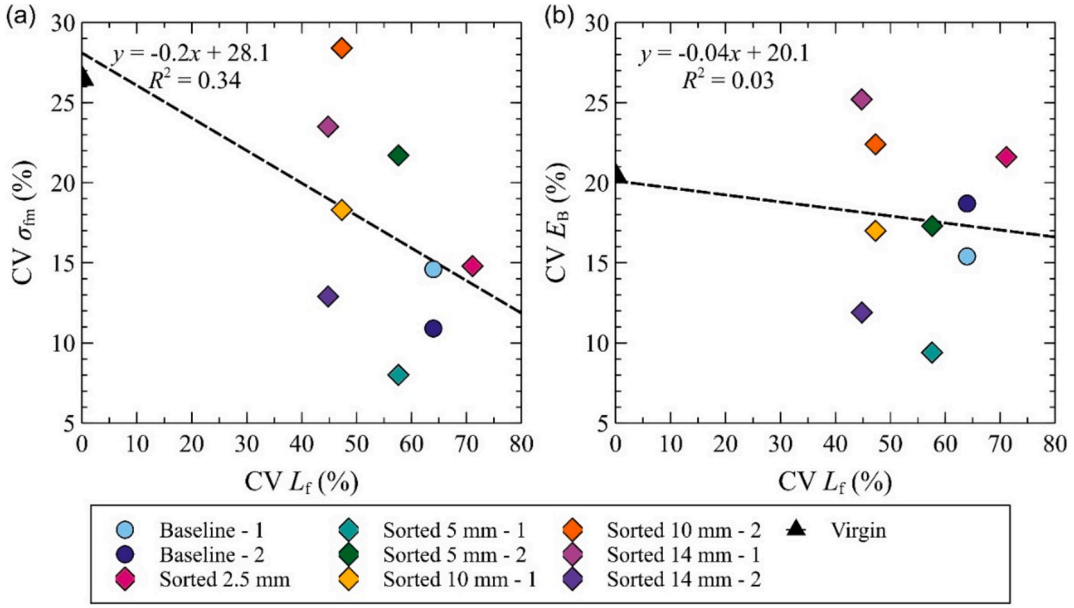

Fig. 25. Evolution of (a) the variation in flexural strength; and (b) modulus relative to the variation in fibre length.

Table 7
Estimated annual TET waste production.

Prepregging Line Usage	Prepreg production capacity (tonnes/yr)	TET waste production for the 609.6 mm (24 in) roll (tonnes/yr)
20 %	64	3.4
40 %	128	6.8
60 %	192	10.2
80 %	256	13.6

prepregging line is estimated between 3.4 and 13.6 tonnes. The Gilson TS-1 screening machine described above is able to process 1 kg of TET waste in 10 min. A similar system may be able to process up to 10 920 kg per year, assuming it runs 35-hour a week and 52 weeks a year. With these conditions, two devices would be required to sieve the maximum waste production at 80 % of line usage for a large 609.6 mm wide roll.

4.2. Greenhouse gas reduction – Environmental impact

The results section highlighted the proximity and sometimes superiority of the tensile and flexural properties obtained using sorted or unsorted TET strands compared to commercial products. The analysis below aims to estimate the greenhouse gas (GHG) emissions that could be saved by reusing TET strands instead of virgin strands. This is not intended to be a life cycle assessment. The study is based on the maximum annual production of TET waste, which is 13.6 tonnes. Two scenarios are considered:

- Scenario 1: 50 % virgin strands and 50 % sorted TET strands
- Scenario 2: 100 % virgin strands

The global warming potential (GWP) is expressed in kg CO_2 eq. The calculations are focused on the first part of a "cradle-to-gate" assessment, *i.e.*, raw materials, with the second part (manufacture) being considered identical for both scenarios. The main source of GHG emissions is related to the production of materials, particularly virgin carbon fibres, which account between 69 % and 87 % of total emissions from panel manufacture [16]. As no data was found for a CF/PEEK prepreg, the emissions used come from Witik's [16] study for one kilogram of CF/epoxy prepreg. Thus, for the entire pre-impregnation process, the associated emissions are 53.6 kg CO2 eq for 1 kg of prepreg. This value is taken as indicative; however, it is important to specify that it could actually be higher depending on the type of fibre (high or standard modulus) and for a thermoplastic matrix. Due to their minimal impact in other studies [16,17] and the lack of comprehensive data for calculations, the emissions associated with cutting operations of virgin prepregs are neglected. The losses related to prepreg manufacturing operations are estimated with the scrap rate of the previous section (5.3 % for the 609.6 mm wide roll) and are included in the calculations. The specifications of the Gilson TS-1 sieving machine are 115 V and 15 A. An electrical consumption of 0.2875 kWh is obtained for the sorting of one kilogram of recycled strands. The emission rate for electricity produced in Québec is 0.62 kg CO2 eq/MWh, as provided by Hydro-Québec [18].

As expected, the main cause of GWP corresponds to the production of prepregs. The sieving process represents barely 0.0003 % of the emissions produced, with a value of 2.4 kg CO2 eq for the 609.4 mm line. Two consequences arise from: the impact of sorting can be neglected when choosing between sorted and unsorted strands. Secondly, the emissions from the mix of virgin and TET strands present a reduction of nearly 50 % in GHG emissions compared to the 100 % virgin scenario. The last scenario is unsurprisingly the most polluting as it involves a whole batch of new materials. By opting to use TET instead of commercial products, approximately 729x10^3 kg of CO2 eq would not be produced yearly, for one prepregging line.

5. Conclusion

This study focused on the sorting of highly variable thermoplastic TET waste recovered from one of Teijin Carbon America Inc.'s aerospace prepreg production lines and the characterisation of the material. Two sieving methods were employed to mechanically separate recovered TET into batches with improved geometric uniformity. The sieving technique using linear vertical motion proved more effective than the horizontal-circular method, offering quicker separation and reducing the tendency for strands to form large aggregates that trapped smaller strands. The Gilson TS-1 sieving system, utilizing linear-vertical motion, was shown to successfully sort 1 kg batches of TET strands within 10 min.

Image analysis and high-speed imaging were used to quantify the geometric characteristics of strands recovered from each sieve, revealing that the minimum strand dimension was the key parameter governing the passage of strands through each sieve. Sieving resulted in batches with notably different average fibre lengths, with the three largest sieves showing lengths greater than those of unsorted strands. Furthermore, sieving reduced variability compared to the original batch of strands by 6.4–28.8 %, with the exception of the TET strands found in the 2.5 mm sieve.

An analysis of the quality of the TET-based compression moulded panels was conducted through non-destructive inspection and microscopy. The areas identified as hotspots were indeed associated with defects, such as porosities, resin-rich zones, fibre swirling, and out-of-plane strands orientations, with the first two being the most common. The mechanical properties were evaluated through tensile and flexural tests, and for both types of tests, the results were characterised by high variability. The hypothesis that strands heterogeneity is the only cause of this variability was rejected, as the analysis of variation coefficients did not indicate a clear trend. An overall increase in tensile and flexural strengths was observed with longer fibre lengths, particularly when comparing widely separated sieve sizes. Stiffness was less influenced by fibre length, consistent with findings from other authors [3,7]. Baseline panels (unsorted strands) produced a range of values encompassing all data obtained from sorted panels. Compared to available literature values, both sorted and unsorted TET strands fell within the same ranges.

Since fibre length variability does not appear to drive the variability in mechanical properties, we conclude that the decision to implement a sorting process should be guided not by the goal of enhancing mechanical performance, but rather by the need to improve the material's formability.

An evaluation of the GHG emissions associated with this solution was carried out. By replacing commercial products with the maximum annual production of TET from one prepregging line, 729 $\times$ 10^3 kg of CO_2 equivalent would be avoided. Given the very low emissions related to sorting for the quantities involved (13.9 tonnes), the use of sorted or unsorted strands should primarily be based on parts geometric constraints.

CRediT authorship contribution statement

A.W. Smith: Writing – original draft, Methodology, Investigation, Formal analysis, Conceptualization. **H. Pattery:** Writing – original draft, Investigation, Formal analysis, Data curation. **J.P. Canart:** Resources, Formal analysis. **I. Tabiai:** Supervision. **M. Dubé:** Writing – review & editing, Supervision, Project administration, Methodology, Funding acquisition, Formal analysis, Conceptualization.

Declaration of competing interest

The authors declare that they have no known competing financial interests or personal relationships that could have appeared to influence the work reported in this paper.

Acknowledgements

The valuable assistance of Dr. Jacques Lengaigne in performing high-speed imaging and with data interpretation is acknowledged. This research was funded by the Marcelle-Gauvreau Research Chair in Environmentally Friendly Composite Materials, Teijin Carbon America Inc., MITACS and the Research Center for High Performance Polymer and Composite Systems (CREPEC).

Appendix A. Supplementary material

Supplementary data to this article can be found online at https://doi.org/10.1016/j.compositesa.2025.109165.

Data availability

Data will be made available on request.

References

[1] Product Data Sheet: Toray Cetex(R) MC1200 PEEK; 2019.
[2] Greene Tweed. Greene Tweed n.d. https://www.gtweed.com/ (accessed July 29, 2024).
[3] Eguémann N, Giger L, Masania K, Dransfeld C, Thiebaud F, Perreux D. Processing and Characterisation of Carbon Fibre Reinforced PEEK with Discontinuous Architecture. 2014.
[4] Feraboli P, Peitso E, Deleo F, Cleveland T, Stickler PB. Characterization of prepreg-based discontinuous carbon fiber/epoxy systems. J. Reinf. Plast. Compos. 2009;28:1191–214. https://doi.org/10.1177/0731684408088883.
[5] Selezneva M, Lessard L. Characterization of mechanical properties of randomly oriented strand thermoplastic composites. J. Compos. Mater. 2016;50:2833–51. https://doi.org/10.1177/0021998315613129.
[6] Yamashita S, Hashimoto K, Suganuma H, Takahashi J. Experimental characterization of the tensile failure mode of ultra-thin chopped carbon fiber tape-reinforced thermoplastics. J. Reinf. Plast. Compos. 2016;35:1342–52. https://doi.org/10.1177/0731684416651134.
[7] Wan Y, Takahashi J. Tensile properties and aspect ratio simulation of transversely isotropic discontinuous carbon fiber reinforced thermoplastics. Compos. Sci. Technol. 2016;137:167–76. https://doi.org/10.1016/j.compscitech.2016.10.024.
[8] Tomblin JS, Andrulonis RM, Lovingfoss RS, Saathoff BL, Ashforth C, Davies C. Characterization approach for compression molded discontinuous fiber thermoplastic composites. SAMPE J 2024;60. https://doi.org/10.33599/SJ.v60no1.02.
[9] Selezneva M, Picher-Martel G-P, Landry B, Trudel-Boucher D, Roy S, Khoun L, et al. Compression moulding of discontinuous-fibre carbon/PEEK composites: Study of mechanical properties. Int SAMPE Tech Conf 2012.
[10] Product Data Sheet: Tenax(R)-E TPUD PEEK-HTS45 2020.
[11] Feraboli P, Cleveland T, Ciccu M, Stickler P, DeOto L. Defect and damage analysis of advanced discontinuous carbon/epoxy composite materials. Compos Part Appl Sci Manuf 2010;41:888–901. https://doi.org/10.1016/j.compositesa.2010.03.002.
[12] Kastner J, Plank B, Salaberger D, Sekelja J. Defect and Porosity Determination of Fibre Reinforced Polymers by X-ray Computed Tomography 2011.
[13] Selezneva M. Experimental and Theoretical Investigations of Mechanical Properties of Randomly-Oriented Strand (ROS) Composites. Ph.D. McGill University (Canada), 2015.
[14] Kravchenko SG, Sommer DE, Denos BR, Favaloro AJ, Tow CM, Avery WB, et al. Tensile properties of a stochastic prepreg platelet molded composite. Compos Part Appl Sci Manuf 2019;124:105507. https://doi.org/10.1016/j.compositesa.2019.105507.
[15] Inside Teijin's thermoplastic tape expansion 2024. https://www.compositesworld.com/articles/inside-teijins-thermoplastic-tape-expansion (accessed July 29, 2024).
[16] Witik RA, Gaille F, Teuscher R, Ringwald H, Michaud V, Månson J-A-E. Economic and environmental assessment of alternative production methods for composite aircraft components. J. Clean. Prod. 2012;29–30:91–102. https://doi.org/10.1016/j.jclepro.2012.02.028.
[17] Bianchi I, Forcellese A, Marconi M, Simoncini M, Vita A, Castorani V. Environmental impact assessment of zero waste approach for carbon fiber prepreg scraps. Sustain. Mater. Technol. 2021;29:e00308. https://doi.org/10.1016/j.susmat.2021.e00308.
[18] Taux d'émission de GES associés à l'électricité | Hydro-Québec n.d. https://www.hydroquebec.com/developpement-durable/documentation-specialisee/taux-emission-ges.html (accessed August 30, 2024).